Journal of Magnetic Resonance **149,** 36–44 (2001)
doi:10.1006/jmre.2001.2284, available online at http://www.idealibrary.com on IDEAL®

MRI-Based D_2O/H_2O-Contrast Method to Study Water Flow and Distribution in Heterogeneous Systems: Demonstration in Wood Xylem

K. Ilvonen,* L. Palva,* M. Perämäki,† R. Joensuu,* and R. Sepponen*

**Applied Electronics Laboratory, Helsinki University of Technology, P.O. Box 3000, 02015 Helsinki, Finland; and †Department of Forest Ecology, University of Helsinki, P.O. Box 24, 00014 Helsinki, Finland*

Received August 1, 2000; revised December 20, 2000

We demonstrate a method for examining water flow and distribution within heterogeneous systems by means of MRI and deuterium oxide (D_2O)/water (H_2O) contrast. In this demonstration a piece of a pine tree was used. In pine xylem, water flows in tube-like dead cells, that is, tracheids, which are about 10–40 μm in diameter and 1–4 mm in length. Water flow in tracheids of a piece of a pine branch was studied by means of D_2O/H_2O contrast obtained with MRI at 1.5 T. D_2O flowing through the object caused reduction of signal when ^1H detection was used. Observed flow velocity in the compression wood was about one-third of that in the tension wood, the former having a smaller average cell lumen size than the latter. After the signal in the entire cross section was reduced to its minimum, the experiment was renewed with distilled H_2O. Flow of the H_2O and hence replacement of D_2O through the wood resulted in the return of the signal. This study demonstrates the dependence of the flow velocity on the cell lumen size. The results suggest that D_2O/H_2O contrast obtained with MRI is an effective tool for studies of water dynamics within heterogeneous systems.

Key Words: **MRI; deuterium oxide (D_2O); contrast indicator; heterogeneous system; water flow.**

INTRODUCTION

There has been wide interest in characteristics of water flow and transport through heterogeneous systems, such as porous media, groundwater filtering systems, aquifers, and soil sediments (*1–6*). MRI techniques, among others, have been used to investigate concentration and velocity field in heterogeneous porous media (*1, 2*), for example.

Cells of a tree form a complex system that takes care of water transportation. The water transportation system and mechanism in different parts of the tree are under extensive research; see, e.g., (*7*). Here we have developed an MRI-based method which can be used to study water flow and distribution in heterogeneous systems. Use of this method has been demonstrated in the water conducting part of a Scots pine (*Pinus sylvestris* L.) trunk, called xylem. The pathway for water flow in the xylem consists of a large number of dead cells, called tracheids, mainly 10–50 μm in diameter and 1–4 mm in length (*8*). The size of the cells varies in different parts of the cross section. For example, the lower part of the tree branch has to carry the weight of the branch; thus in this area of the cross section, called compression wood, cell walls are thicker and cell lumens are smaller than those in the upper part of the branch cross section, called the tension wood. Openings, called pits, which are 6–20 μm in diameter (*9*), connect a cell to other cells.

Mechanics of water transportation in conifers has been studied, for example, by injecting dye into the tree and then cutting it into pieces to follow the path of the dye (*10, 11*). Also, other methods like radio- and stable isotopes (*12*), poto- and lysimeters (*13*), and thermal methods have been used. Thermal methods, i.e., heat pulse velocity (HPV) (*13–15*) and heat balance (*13, 16–19*), are based on either pulsating or continuous heating of the trunk and then recording the temperature rise at a specified distance. However, in pine trees, the well-defined ring structure gives rise to a complex radial pattern of sap flow (*14*), which is not yet fully understood. Dye *et al*. showed that HPV sap flow values consistently overestimated water uptake because the heat is also conducted to areas that do not transport water (*14*).

One possibility is to use MRI for water flow studies. Some benefits of MRI are its noninvasive and nondestructive nature. Very high in-plane resolution can be achieved if a high field imaging system is used (*20*). However, the structure of pine makes MR imaging more complicated than imaging of smaller plants having simpler structures. Therefore, it is easier to achieve satisfactory resolution with smaller plants and they have been used as the object of research. Several NMR and MRI studies of fruits, vegetables, and other plants have been reported (*21–34*). For example, *in situ* water balance studies of a cucumber plant (*21*) and water flow in maize (*22*) have been demonstrated. The water content of a kiwifruit (*23*) and a coconut (*24*) has also been studied. MRI-based diffusion and flow measurements have been performed, for example, with castor bean (*25*) and rough horsetail (*26*). However, to the best of our knowledge, there have been only a few MRI studies of wood (*35–38*).

Our unpublished measurements with fresh, water-filled pieces of a pine show that, at 1.5 T, T1 and T2 proton relaxation times in a pine are relatively short, from 50 to 200 ms and from 10 to 60 ms, respectively. The relaxation times indicate that a large part of the water in a pine is strongly bound to the wood material.

1090-7807/01 $35.00

Moreover, the size of the tracheids varies within the annual rings and also between different areas of the pine. Therefore, the relaxation times can largely vary between different parts of the tree, depending on the cell size and water contents.

There are a few MRI methods that can be used to study water flow. One is the phase-contrast method, where the velocity information is encoded in the phases of the precessing spins. Although the phase-contrast method has been used in several applications, in the case of a tree this approach might not be so beneficial due to the slow flow velocity and signal level. Different methods will be compared under Discussion. The time-of-flight (TOF) method, where movements of saturated spins of the fluid are followed, could be possible. However, due to short T1 this probably is not a very effective method. One possibility is to use deuterium oxide (D_2O) as an indicator. Deuterium, having paired spins, gives no NMR signal when ^1H detection is used. Deuterium oxide has been used previously to study signal intensity-based H_2O–D_2O water exchange in roots of a maize seedling (*20*). In our experiment, D_2O has been used to achieve negative contrast, i.e., signal void. After the signal has reached its minimum, H_2O has been used as an indicator to achieve positive contrast, i.e., signal return. This method enables full exploitation of maximum signal and contrast. The purpose of the study is to develop and demonstrate the feasibility of an MRI-based method that can be used to study water flow velocity and water distribution within heterogeneous systems. Here, an MRI-based D_2O/H_2O-contrast method is suggested to fulfill this purpose.

MATERIALS AND METHODS

Pieces of a pine were received from the Helsinki University SMEAR II (*39*) forest research station, located at Hyytiälä, central Finland. The sample piece selected for measurement was taken from a branch of a pine about 7 years old. The diameter of the piece was about 17–19 mm including the bark and it was about 20 cm in length. It was stored in a sealed plastic bag under water. Images were obtained within 24 h after cutting the piece from the pine. Here the effects of osmotic pressure is not of concern, since water conducting pipes in xylem are dead (*7, 8, 40*). Furthermore, the use of a sample piece and distilled water is a standard procedure as indicated in Refs. (*41–43*).

Measurements were performed at 1.5 T (63.5 MHz for ^1H) with a whole-body human scanner (Vision, Siemens, Germany). The signal coil used was a loop 30 mm in diameter. Water was directed into the pine with a silicone hose. One end of the piece of pine was inside the hose and the other end was inside a chamber, where liquids coming through the pine were collected. The D_2O used was 99.99% pure (Aldrich Chemical Co. Inc., Germany) and distilled water, H_2O, was obtained from the Helsinki University of Technology, Department of Chemistry. The measurement setup is shown in Fig. 1.

A 3D sequence called constructive interference in steady state (CISS) (*44*) was used with the parameters TE = 5.9 ms, TR = 12.25 ms, flip angle 70°, matrix 256 × 256, and FOV

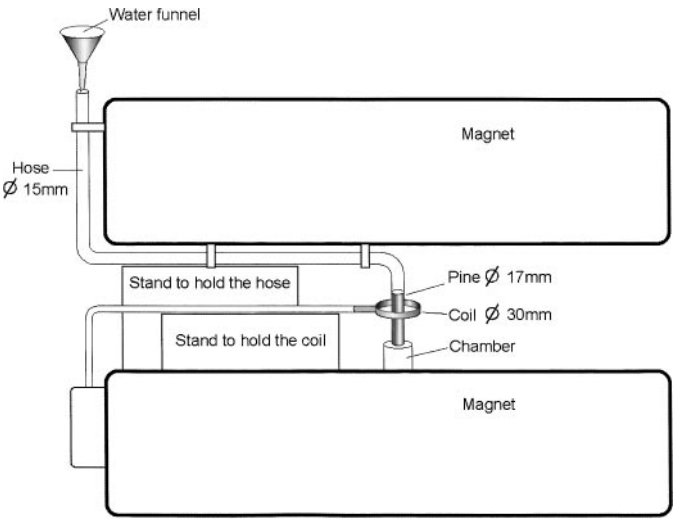

FIG. 1. Arrangement for measuring D_2O/H_2O flow within a pine at 1.5 T.

80 mm, resulting in the plane pixel size 0.31 × 0.31 mm. A 32-mm-thick 3D slab consisting of 32 slices with an effective thickness of 1 mm was collected. The total scan time for one slab was 3 min 22 s. In a cross-sectional plane, one pixel covers more than 100 wood cells. A short TR was used to maintain the steady state.

Reference images were first acquired. About 3 dl of D_2O was added to the hose. Scanning was performed repeatedly every fourth minute until the signal from the imaging volume seemed to reach a minimum intensity, which took about 160 min. Then the remaining D_2O was removed from the feeding hose, and distilled water was added 178 min after the beginning of the experiment. Images were taken, as explained above, until the signal returned, which took about 110 min. The diminishing of the signal was slower than the increasing of the signal because there was less D_2O available; i.e., the pressure in the hose was not as high that with H_2O.

Optical microscope images of selected areas of the studied pieces of a pine were taken after the experiment. These images were prepared by the Botanical Museum of the University of Helsinki. The sizes of the cell lumen were analyzed from these microscope images with an image analyzer program (Colorsoft Oy, Helsinki, Finland).

RESULTS

The study of the results is divided into three parts. First, one cross-sectional slice from the most homogeneous area, i.e., from the middle of each slab, is examined. In this analysis we follow signal intensity changes in selected areas of the cross section. Second, we examine microscope images taken from the piece of pine under study. Third, intensity changes in longitudinal images are recorded. This analysis enables us to calculate absolute flow velocities in the imaged object.

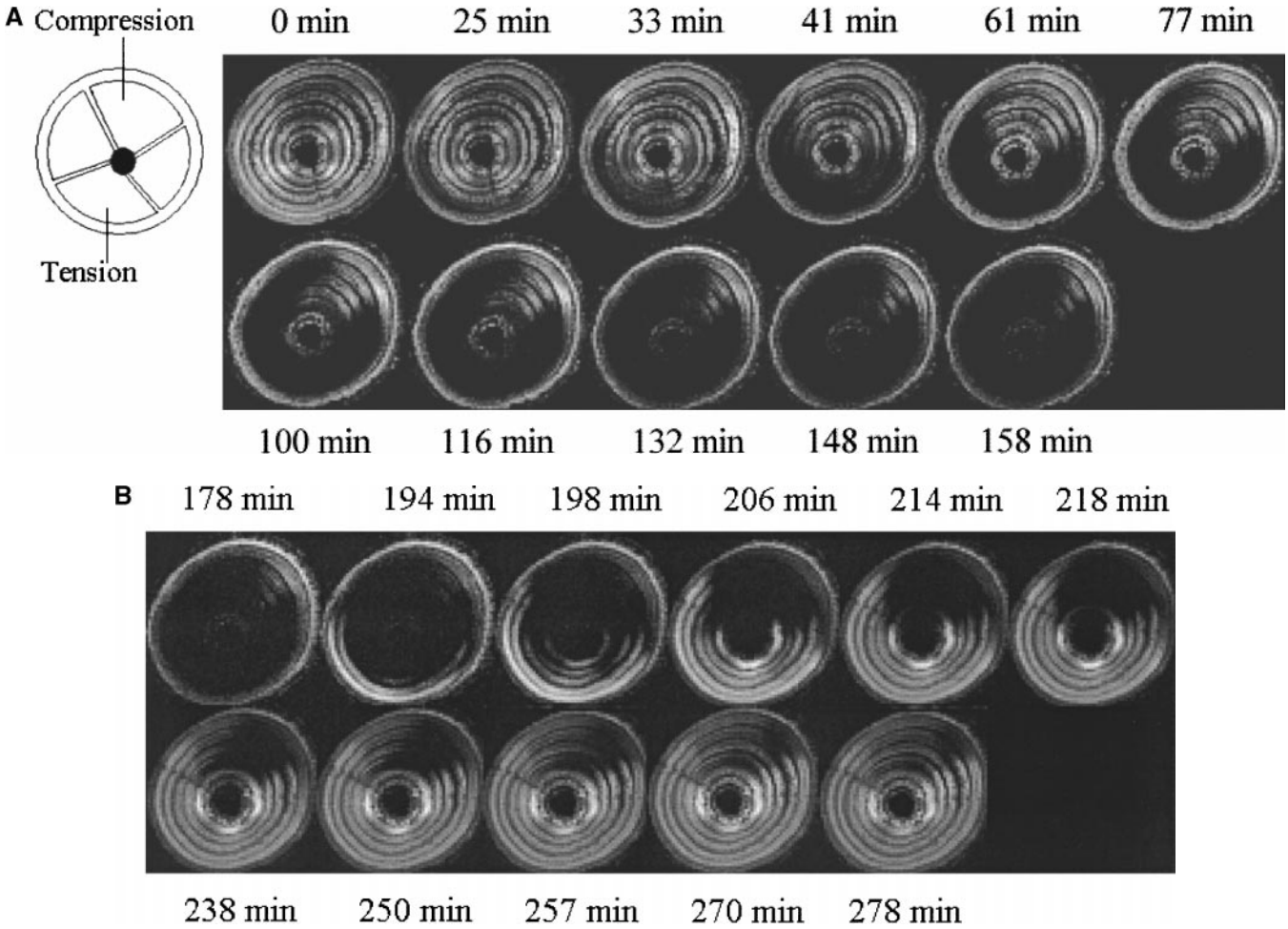

FIG. 2. Time series of an enlargement of a cross-sectional image showing D_2O (A) and H_2O (B) flow through the piece of a pine. Signal diminishing (A) demonstrates the flow of D_2O and signal increasing (B) the flow of H_2O. D_2O was added at 0 min and H_2O at 178 min. 3D CISS sequence, slab of 32 slices 1 mm each, TR/TE 12.25/5.9 ms, matrix 256 × 256, FOV 80 mm. Here only the middle slice of the slab is shown.

Enlargements of the cross-sectional images, at selected times after D_2O was added, are shown in Fig. 2A. Similarly, Fig. 2B shows enlargements of the cross-sectional images in time series after H_2O was added. It can be seen from the figures that both H_2O and D_2O pass faster through the tension wood than the compression wood. Microscope images, Figs. 3A–3C, reveal that there are significant differences in the structure of these two areas. The average cell lumen diameter weighted by the amount of cells is 13 and 18 μm in the compression and tension wood, respectively. The largest cells in the analyzed images have diameters of 26 μm in the compression wood and 40 μm in the tension wood. Figure 4 presents the cumulative share of the total lumen area as a function of lumen size class. As can be seen from the graph, in the compression wood, the distribution of cells is weighted around 200 μm^2, whereas in the tension wood it is around 450 μm^2. Thus, this method enables us to relate average flow velocity to the average cell lumen size.

If we focus on the four areas of the cross section whose average intensity as a function of time is shown in Fig. 5, we can point out a few other findings. The most prevalent finding is that used indicator liquids give a good contrast, as shown in Fig. 5; the signal intensity drops to a few percentage points of its original value. At the beginning, the relative intensity in the compression wood area is almost one-third of the intensity in the tension wood area. The situation is similar at the end of the measurement. However, the signal does not return to its original value in any of the areas. It can be seen from Fig. 5 that the average signal intensity decreases and increases in the tension wood about three times faster than in the compression wood.

Using 3D imaging enables us to reconstruct longitudinal images of the object. These images provide the possibility to investigate absolute flow velocities in different parts of the pine. Figure 6A shows a time series of longitudinal images after D_2O was added. A similar time series after adding H_2O is presented in Fig. 6B. The dark area in the middle of the images is the pith. First, we investigate average intensity changes along a vertical line covering partially the tension wood of slices 22 and 13, 1 cm apart from each other, by means of a time derivative of the

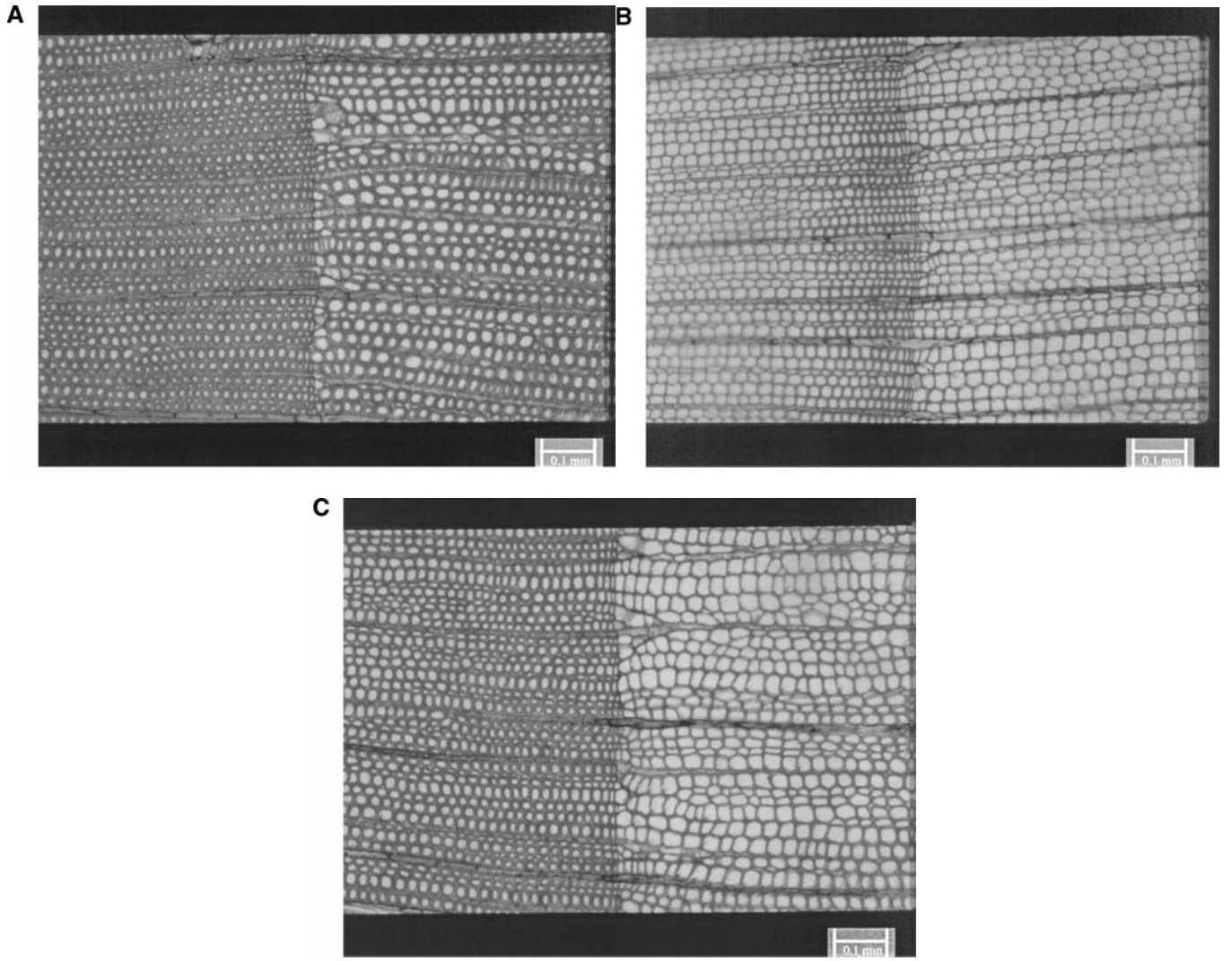

FIG. 3. Light microscope image at the border of the sixth and seventh annual ring in the compression (A) and tension (B) wood of the pine. Image C is taken at the border of the sixth and seventh annual ring between the compression and tension wood areas (1 : 128).

average intensity. This derivative is shown in Fig. 7A as a function of time. It can be noticed that there is a peak in the derivative of intensity in slice 22 at time 24 min, whereas in the derivative of intensity in slice 13, the peak is at time 32 min. If bulk-type flow is assumed, we can approximate the average flow velocity in this part of the tension wood to be about 7.5 cm/h. However, when the derivative of the intensity in the compression wood was examined, there were no differing peaks or clear maximum or minimum, but the intensity seemed to change quite rapidly without any clear trend as shown in Fig. 7B.

Next, we examine the intensity profile along a longitudinal line in both tension and compression wood areas because the absolute flow velocity in compression wood could not be calculated by means of a derivative of the intensity. One pixel width longitudinal line, which covers all 32 slices, is under study. Examination starts when the intensity has reached its minimum and begins to increase due to H_2O inflow after 178 min. As shown in Figs. 8A and 8B, the signal intensity in wood is close to zero in all slices at this time interval. Figure 8A shows the intensity profile along one longitudinal line approximately in the middle of the compression wood at different times after H_2O inflow. In this figure, the water flow is from right to left. It can be observed

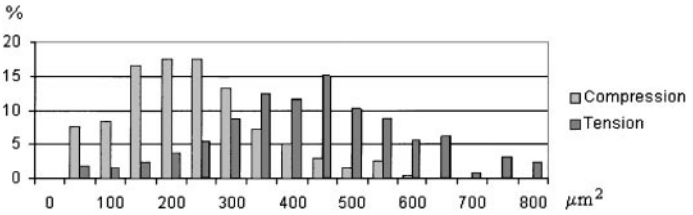

FIG. 4. Cumulative share [%] of the total lumen area as a function of lumen cell size class [μm^2] from the samples of the tension and the compression woods of the imaged pine.

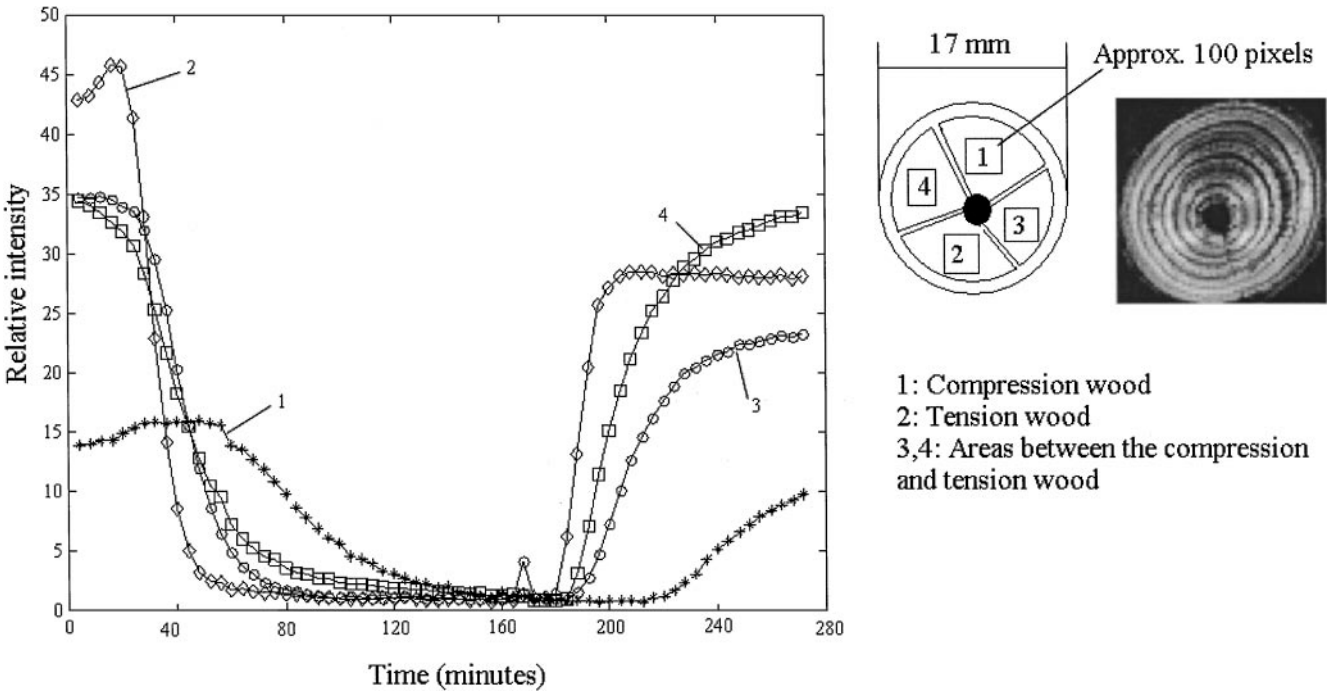

FIG. 5. Average intensity in four different areas of the cross section as a function of time. Average intensity is shown in relative units.

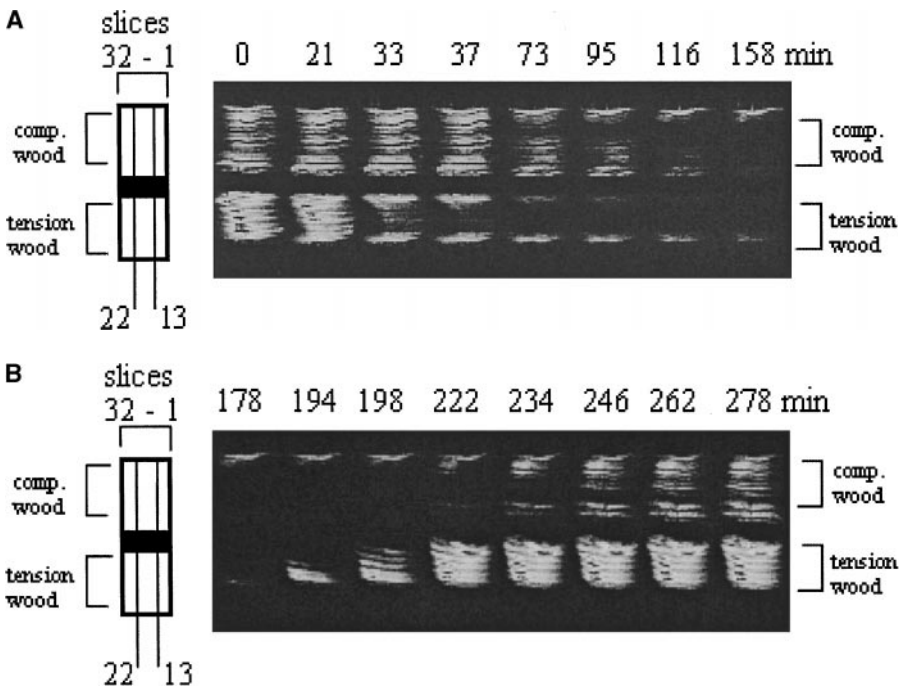

FIG. 6. Time series of the longitudinal image of the piece of a pine. The time scale is from the beginning of the experiment. Water flow from left to right can be seen as the signal diminishes (A) and increases (B). D_2O was added at 0 min (A) and H_2O at 178 min (B). These images have been computably reconstructed from acquired 3D slabs, partly shown in Fig. 2.

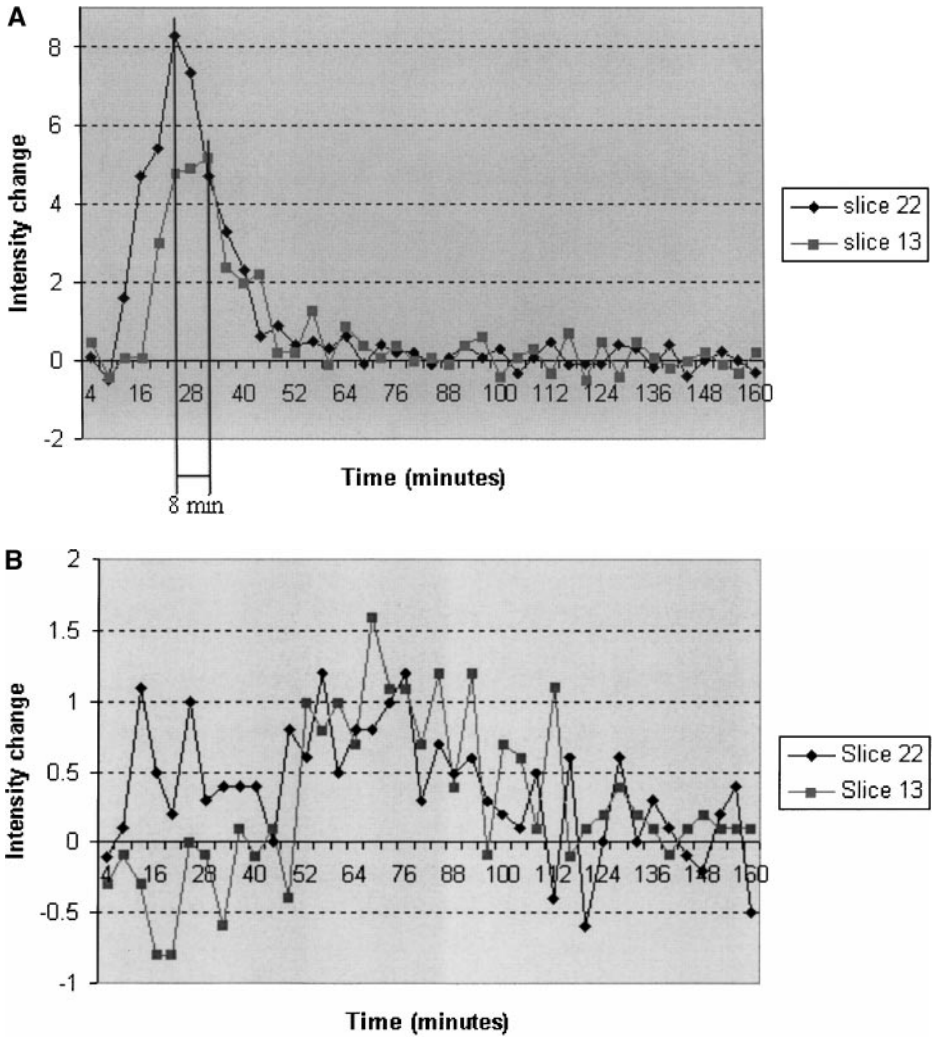

FIG. 7. Derivative of the average intensity in tension (A) and compression (B) wood in slices 22 and 13 as a function of time during D_2O inflow.

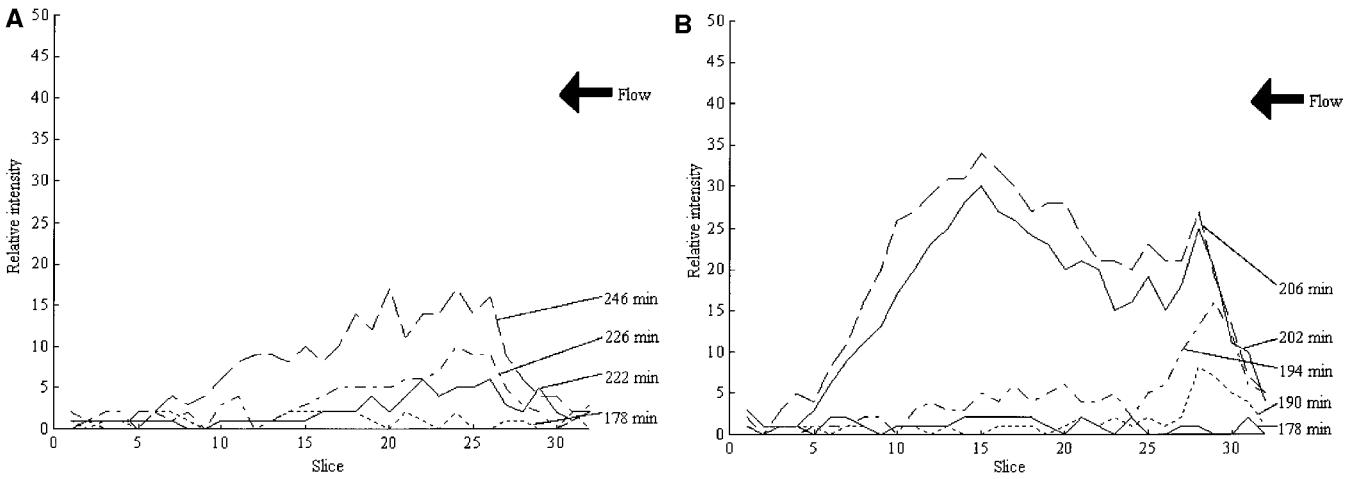

FIG. 8. Average intensity during H_2O inflow along one pixel width longitudinal line in the compression (A) and tension (B) wood at selected time intervals. Water flow is from right to left. H_2O was added at 178 min.

that the intensity in slice 10 at time 246 min has increased to the same value as the intensity at time 226 min in slices 25. The distance between slices 25 and 10 is 1.6 cm. On the basis of this information, we can estimate transient flow velocity in this part of the compression wood to be 4.8 cm/h. A similar situation along one longitudinal line in the tension wood is shown in Fig. 8B. The distance between slices 29 and 10 is 2 cm and it takes about 8 min for the intensity to increase in slice 10 to the same value as in slice 29 at time 194 min. Momentary flow velocity can be approximated to be 15 cm/h in this part of the tension wood.

DISCUSSION

We discuss three main results: (1) The method presented enables us to follow water flow in different kinds of heterogeneous cell populations, in xylem of a pine in this case, in the scale of tens of micrometers. Relative flow velocities in four areas of the cross section of pine, each about 3×3 mm in size, have been recorded. Analysis of Fig. 5 allows us to compare flow velocities in the tension and compression woods and to relate the average flow velocity to the average cell lumen size. Intensity changes and differences in flow velocities in the four areas can be seen clearly from this figure.

It may be noticed from Fig. 5 that the signal intensity does not return to its original value. One probable reason is that at the beginning of the experiment the pine branch was in its natural environment, i.e., filled with water taken up by the roots of the tree. However, at the end of the experiment it was filled with distilled water. Use of distilled water flushes away particles from wood cells, thus changing relaxation times and signal intensity. Deuterium oxide can probably bind to the cell walls and consequently diminish the signal in the signal return phase. The return of the signal could have been improved by flushing longer with H_2O. This effect could have been studied by filling the pine piece with distilled water at the beginning of the experiment and then using D_2O for signal void and H_2O for signal return.

(2) The derivative of the average intensity in selected parts of the tension and compression wood areas was examined as shown in Figs. 7A and 7B. Clear peaks in Fig. 7A justify the assumption of bulk type of flow and enable us to estimate flow velocity from the derivative of the average intensity. However, as can be seen from Fig. 7B, there are no differing peaks and flow velocity in the compression wood cannot be calculated based on this information. Such a result indicates that in the compression wood flow velocities are distributed; thus the derivative cannot be defined. The reason for this observation is that there are several differences in the tension and compression wood tissues, such as differences in cell sizes and shorter tracheids (*45*), as well as more pits in the compression wood (*39, 46*). Shorter tracheids and a larger number of pits cause more tracheid-to-tracheid passages and thus more flow resistance in the compression wood. Because larger cells are dominant in the tension wood, as shown in Fig. 4, inflow of D_2O takes place first in them and this is sufficient to make the signal intensity drop. However, in the compression wood, the inflow of D_2O in large cells does not cause such a rapid fall in the signal intensity, because of the small amount of such cells. Thus, signal intensity does not reach the minimum until D_2O has also passed through the smaller cells.

(3) By analyzing the intensity profiles along one longitudinal line, as shown in Figs. 8A and 8B, we were able to calculate transient flow velocities in both compression and tension wood. Distribution of flow velocities in selected parts of the water conduction system can be examined by analyzing a number of lines.

Next, we compare the D_2O/H_2O-contrast method with other MRI-based methods: paramagnetic contrast agents and phase-encoding methods. As results show, we were able to achieve very good contrast with D_2O. When compared with paramagnetic contrast agents, such as $MnCl_2$; one advantage of D_2O is its chemical similarity to H_2O. Another advantage of D_2O is that the use of special pulse sequences optimized for D_2O is not required. Possible change of T1 and T2 relaxation times due to D_2O is not of concern here, since the contrast is determined by the ratio of these two relaxation times, which is fairly constant.

Despite the fact that the phase-contrast method is suitable in several applications, in our unpublished studies we have noticed that, in the case of a tree, poor signal level hampers the use of this method for flow imaging. A short $T2^*$ indicates that microscopic spatial changes of the magnetic field are present in wood material. The D_2O/H_2O-contrast method is insensitive to these effects. If we use a clinical MRI system and apply the phase-contrast method, we have to use a large voxel size to acquire enough signal at the expense of resolution. With the D_2O/H_2O-contrast method we have also maximized signal intensity and contrast, unlike in the phase-encoding method. Another disadvantage of the phase-encoding method is that very powerful and fast gradients are needed, due to slow flow velocity, to achieve sufficiently high phase differences.

Heat pulse velocity (HPV) has been shown to be a useful method for measuring flow in several hardwoods (*14*). However, the HPV method has not been sufficiently verified for softwoods, because of the structure of softwood that gives rise to a complex radial flow (*14*). Even though Dye *et al*. (*14*) mention minimal disturbance as an advantage of the HPV method, heating of the trunk of a tree as well as inserting probes inside the trunk might have an effect on its function. When compared with the HPV method, one advantage of the D_2O/H_2O-contrast method is that we can also follow the water pathway and distribution in areas with different cell sizes and we are able to localize nonconducting parts of the trunk. Parts that do not conduct water conduct heat and thus cause errors in the HPV method. Another widely used method is to inject dye into the tree and follow its pathway by cutting the tree into pieces after the experiment. Unlike MRI, this simple and reliable method always requires the cutting of the tree and only the pathway of the water can be followed, not the flow velocity in different parts of the trunk.

In a controlled system, the effect of environmental factors on the water flow in an intact sapling could be noninvasively

studied. Changes in temperature or lighting conditions, for example, will affect the water flow and variations could be followed. For example, Van As *et al*. (*21*) have imaged an intact cucumber plant in a controlled climate chamber. The system presented in their paper is applicable to plants with diameter under 1 cm due to the bore size of the magnet. However, in principle such an arrangement is possible for larger plants also.

Because D_2O gives good contrast, it might be possible to study the effect of embolism and tissue damage to the water flow in a pine if we have sufficient resolution compared with the size of the damaged area. The D_2O/H_2O-contrast method could be improved by using better resolution and shorter imaging times. However, these parameters are partly related to the factors of the imaging system used. In this research, the measurement time limited observations to every fourth minute. However, it seemed to be sufficient because of the slow flow velocity in coniferous trees.

CONCLUSIONS

To the best of our knowledge, this is the first MRI-based method which can be applied noninvasively to study water dynamics including very slow flow velocity and to visualize the water flow in different parts of the tree and in different kinds of cell populations with high precision. On the basis of this demonstration we can draw the conclusion that water flow and distribution within trees can be effectively investigated with MRI by means of H_2O and D_2O as contrast indicators. This method enables us to maximally utilize signal intensity and contrast. Results demonstrate that water flow in a pine can be followed with this method and flow velocity may be related to the cell lumen size. Absolute velocities can be recorded and relative velocities and distribution can be clearly demonstrated. The D_2O/H_2O-contrast method will open new vistas in studies of water dynamics in wood material and in other heterogeneous systems.

ACKNOWLEDGMENTS

We thank Ms. T. Timonen and Ms. P. Harju (Botanical Museum, University of Helsinki) for preparation of the microscope images and Colorsoft Oy for analyzing these images. Ms. Ilvonen thanks the Finnish Cultural Foundation and Foundation of the Association of Electrical Engineers in Finland for grants. Dr. Palva and Ms. Ilvonen thank the Foundation of the Finnish Society of Electronics Engineers for grants.

REFERENCES

1. N. C. Irwin, S. A. Altobelli, and R. A. Greenkorn, Concentration and velocity field measurements by magnetic resonance imaging in aperiodic heterogeneous porous media, *Magn. Reson. Imaging* **17**(6), 909–917 (1999).
2. M. Y. Su and O. Nalcioglu, Susceptibility effects in porous media in the presence of flow. *J. Magn. Reson. Imaging* **3**(5), 794–799 (1993).
3. A. Keller, High resolution, non-destructive measurement and characterization of fracture apertures, *Int. J. Rock Mech. Mining Sci.* **35**(8), 1037–1050 (1998).
4. H. J. Bertin, O. G. Apaydin, L. M. Castanier, and A. R. Kovscek, Foam flow in heterogeneous porous media: Effect of crossflow, *Proc. Spe. Symp. Improv. Oil Recovery, Soc. Pet. Eng. (Spe), Richardson, TX (USA)* **2,** 255–264 (1998).
5. D. V. Chitale, P. I. Day, and G. R. Coates, Petrophysical implications of laboratory NMR and petrographical investigation on a shaly sand core, *Proc. Spe. Annu. Tech. Conf. Exhib., Soc. Pet. Eng. (Spe), Richardson, TX (USA)* **Omega**, 607–615 (1999).
6. P. D. Majors, P. Li, and E. J. Peters, NMR imaging of immiscible displacements in porous media, *Proc. Spe. Annu. Tech. Conf. Exhib., Soc. Pet. Eng. (Spe), Richardson, TX (USA)* **Omega**, 263–278 (1995).
7. M. J. Canny, Transporting water in plants, *Am. Sci.* **86,** 152–159 (1998).
8. M.-S. Ilvessalo-Pfäffli, "Fiber Atlas, Identification of Papermaking Fibers," Springer-Verlag Berlin/New York (1995).
9. J. F. Siau, "Wood: Influence of Moisture on Physical Properties," Department of Wood Science and Forest Products, Polytechnic Institute and State University (1995).
10. J. P. Vité and J. A. Rudinsky, The water-conducting systems in conifers and their importance to the distribution of trunk injected chemicals, *Contrib. Boyce Thompson Inst.* **20,** 27–38 (1959).
11. E. Nikinmaa, L. Kaipiainen, M. Mäkinen, J. Ross, and T. Sasonova, Geographical variation in the regularities of woody structure and water transport, *Acta Forest. Fennica* **254,** 49–78 (1996).
12. P. W. Owston, J. L. Smith, and H. G. Halverson, Seasonal water movement in tree stems, *Forest Sci.* **18**(4), 266–272 (1972).
13. S. D. Wullschleger, F. C. Meinzer, and R. A. Vertessy, A review of whole plant water use studies in trees, *Tree Physiol.* **18**(8/9), 499–512 (1997).
14. P. J. Dye, S. Soko, and A. G. Poulter, Evaluation of the heat pulse velocity method for measuring sap flow in *Pinus patula. J. Exp. Bot.* **47**(300), 975–981 (1996).
15. B. J. Miller, P. W. Clinton, G. D. Buchan, and A. B. Robson, Transpiration rates and canopy conductance of *Pinus radiata* growing with different pasture understories in agroforestry systems, *Tree Physiol.* **18**(8/9), 575–582 (1998).
16. N. Phillips, R. Oren, and R. Zimmermann, Radial patterns of xylem sap flow in non-, diffuse- and ring-porous tree species, *Plant, Cell Environ.* **19**(8), 983–990 (1996).
17. G. E. Jackson, J. Irvine, and J. Grace, Xylem cavitation in Scots pine and Sitka spruce saplings during water stress, *Tree Physiol.* **15**(12), 783–790 (1995).
18. J. Cermak, E. Cienciala, J. Kucera, A. Lindroth, and E. Bednarova, Individual variation of sap-flow rate in large pine and spruce trees and stand transpiration: A pilot study at the central NOPEX site, *J. Hydrol.* **168**(1/4,) 17–27 (1995).
19. M. Perämäki, T. Vesala, and E. Nikinmaa, Analysing the applicability of the heat balance method for estimating sap flow in boreal forest conditions, *Boreal Environ. Res.*, in press (2001).
20. A. Connelly, J. A. B. Lohman, B. C. Loughman, H. Quiquampoix, and R. G. Ratcliffe, High resolution imaging of plant tissues by NMR, *J. Exp. Bot.* **38,** 1713–1723 (1987).
21. H. Van As, J. E. A. Reinders, P. A. de Jager, P. A. C. M. van de Sanden, and T. J. Schaafsma, *In situ* plant water balance studies using a portable NMR spectrometer, *J. Exp. Bot.* **45,** 61–67 (1994).
22. E. Kuchenbrod, M. Landeck, F. Thümer, A. Haase, and U. Zimmermann, Measurement of water flow in the xylem vessels of intact maize plants using flow sensitive NMR imaging, *Bot. Acta* **109,** 184–186 (1996).
23. P. T. Callaghan, C. J. Clark, and L. C. Forde, Use of static and dynamic NMR microscopy to investigate the origins of contrast in images of biological tissues, *Biophys. Chem.* **50,** 225–235 (1994).

24. N. R. Jagannathan, V. Govndaraju, and P. Raghynathan, In vivo magnetic resonance study of the histochemistry of coconut (*Cocos nucifera*), *Magn. Reson. Imaging* **13,** 885–892 (1995).

25. F.-W. Bentrup, NMR-microscopy: Observing xylem and phloem conduits at work, *Bot. Acta* **109,** 177–179 (1996).

26. Y. Xia, V. Sarafis, E. O. Campbell, and P. T. Callaghan, Noninvasive imaging of water flow in plants by NMR microscopy, *Protoplasma* **173,** 170–176 (1993).

27. M. Rokitta, U. Zimermann, and A. Haase, Fast NMR flow measurements in plants using FLASH imaging, *J. Magn. Reson.* **137,** 29–32 (1999).

28. A. V. Anismov, N. Y. Sorokina, and N. R. Dautova, Water diffusion in biological porous systems: A NMR approach, *Magn. Reson. Imaging* **16,** 565–568 (1998).

29. H. C. W. Donker, H. Van As, H. J. Snijder, and H. T. Edzes, Quantitative ^{1}H-NMR imaging of water in white button mushroom (*Agaricus bisporus*), *Magn. Reson. Imaging* **15,** 113–121 (1997).

30. U. Zimmermann, A. Haase, D. Langbein, and F. Meinzer, Mechanisms of long-distance water transport in plants: A re-examination of some paradigms in the light of new evidence, *Philos. Trans. R. Soc. London B Biol. Sci.* **341,** 19–31 (1993).

31. G. A. Johnson, J. Brown, and P. J. Kramer, Magnetic resonance microscopy of changes in water content in stems of transpiring plants, *Proc. Natl. Acad. Sci. USA* **84,** 2752–2755 (1987).

32. H. C. W. Donker, H. Van As, H. T. Edzes, and A. W. H. Jans, NMR imaging of white button mushroom (*Agaricus bisporis*) at various magnetic fields, *Magn. Reson. Imaging* **14,** 1205–1215 (1996).

33. B. P. Hills and S. L. Duce, The influence of chemical and diffusive exchange on water proton transverse relaxation in plant tissues, *Magn. Reson. Imaging* **8,** 321–331 (1990).

34. T. W. J. Scheenen, D. van Dusschoten, P. A. de Jager, and H. Van As, Microscopic displacement imaging with pulsed field gradient turbo spin-echo NMR, *J. Magn. Reson.* **142,** 207–215 (2000).

35. L. D. Hall, V. Rajanayagam, W. A. Stewart, and P. R. Steiner, Magnetic resonance imaging of wood, *Can. J. For. Res.* **16,** 423–426 (1986).

36. L. D. Hall, V. Rajanayagam, W. A. Stewart, P. R. Steiner, and S. Chow, Detection of hidden morphology of wood by magnetic resonance imaging, *Can. J. For. Res.* **16,** 684–687 (1986).

37. P. Millard and J. A. Chudek, Imaging the vascular continuity of *Prunus avium* petioles during leaf senescence using nuclear magnetic resonance spectroscopy, *J. Exp. Bot.* **44**(260), 599–603 (1993).

38. R. S. Menon, A. L. MacKay, S. Flibotte, and J. R. T. Hailey, Quantitative separation of NMR images of water in wood on the basis of T2, *J. Magn. Reson.* **82,** 205–210 (1989).

39. T. Vesala, J. Haataja, P. Aalto, N. Altimir, G. Buzorius, E. Garam, K. Hämeri, H. Ilvesniemi, V. Jokinen, P. Keronen, T. Lahti, T. Markkanen, J. M. Mäkelä, E. Nikinmaa, S. Palmroth, L. Palva, T. Pohja, J. Pumpanen, Ü. Rannik, E. Siivola, H. Ylitalo, P. Hari, and M. Kulmala, Long-term field measurements of atmosphere–surface interactions in boreal forest combining forest ecology, micrometeorology, aerosol physics and atmospheric chemistry, *Trends Heat Mass Moment. Transf.* **4,** 17–35 (1998).

40. M. H. Zimmermann, "Xylem Structure and the Ascent of Sap," Springer-Verlag, Berlin/New York (1983).

41. M. Mecuccini, J. Grace, and M. Fioravanti, Biomechanical and hydraulic determinants of tree structure in Scots pine: Anatomical characteristics, *Tree Physiol.* **17,** 105–113 (1997).

42. W. R. N. Edwards and P. G. Jarvis, Relations between water content, potential and permeability in stems of conifers, *Plant Cell Environ.* **5,** 271–277 (1982).

43. J. J. Sperry, J. R. Donnelly, and M. T. Tyree, A method for measuring hydraulic conductivity and embolism in xylem, *Plant Cell Environ.* **11,** 35–40 (1987).

44. M. Deimling and G. Laub, Constructive interference in steady state (CISS) for motion sensitivity reduction, *in* Abstracts of the Society of Magnetic Resonance in Medicine, 8th Annual Meeting, Amsterdam, p. 842 (1989).

45. M. Kärkkäinen, "Puutiede (Wood Science)," Sallisen kustannus, Sotkamo (1985). [In Finnish]

46. J. Sirviö and P. Kärenlampi, Pits as natural irregularities in softwood fibers, *Wood Fiber Sci.* **30**(1), 27–39 (1998).